Frost, Ray and Weier, Matt and Martens, Wayde and Kristof, Janos (2005) Thermo-Raman spectroscopic study of the uranium mineral sabugalite. *Journal of Raman Spectroscopy* 36(8):797-805.

Thermo-Raman spectroscopic study of the uranium mineral sabugalite

Ray L. Frost [a•], Matt L. Weier [a], Wayde N. Martens [a] and János Kristóf [b]

[a] Inorganic Materials Research Program, School of Physical and Chemical Sciences, Queensland University of Technology, GPO Box 2434, Brisbane Queensland 4001, Australia.

[b] Department of Analytical Chemistry, University of Veszprém, H8201 Veszprém, P.O. Box 158, Hungary.

Abstract

The changes in the structure of sabugalite have been undertaken using thermo-Raman and infrared spectroscopy based upon the results of thermogravimetric analysis. Two Raman bands are observed at 835 and 830 cm^{-1} assigned to the $(UO_2)^{2+}$ stretching vibrations resulting from the non-equivalence of the uranyl bonds $(UO_2)^{2+}$. These bands give calculated U-O bond lengths of 1.773 and 1.7808 Å. A low intensity band is observed at 895 cm^{-1} assigned to the ν_3 antisymmetric stretching vibration of $(UO_2)^{2+}$ units. Five bands are observed in the 950 to 1050 cm^{-1} region in the Raman spectrum of sabugalite and are assigned to the ν_3 antisymmetric stretching vibration of $(PO_4)^{3-}$ units. Changes in the Raman spectra reflect changes in the structure of sabugalite as dehydration occurs. No $(PO_4)^{3-}$ symmetric stretching mode is observed. This result is attributed to the non-equivalence of the PO bonds in the PO_4 units. The PO_4 vibrations were not affected by dehydration. Thermo-Raman spectroscopy proved to be a very powerful technique for the study of the changes in the structure of sabugalite during dehydration.

Keywords: autunite, sabugalite, phosphate, dehydration, Raman spectroscopy, infrared spectroscopy

Introduction

Uranyl phosphates and arsenates are widespread in parts of Australia [1] and are known as members of the autunite group of minerals and were formerly known as the uranyl micas and constitute one of the largest and most widespread groups of uranium minerals. [2] The minerals have a general formula $M(UO_2)_2(XO_4)_2.8\text{-}12H_2O$ where M may be Ba, Ca, Cu, Fe^{2+}, Mg, Mn^{2+} or ½(HAl) and X is As, or P. In this mineral group there are also minerals based upon univalent cations. These include metaankoleite (K), uramphite (NH_4), and sodium uranospinite (Na). Autunites are common minerals, yet have been not often studied in terms of vibrational spectroscopy and rarely in terms of Raman spectroscopy. [3-7] The minerals have a layer-like structure in which uranium is bound in uranyl phosphate or uranyl arsenate layers.[3,8,9]. The minerals lend themselves to Raman spectroscopy because of the low temperatures of dehydration and because all of the molecular components (UO_2, PO_4, AsO_4, H_2O) will be characteristically both Raman and infrared active. The cations and water are located in the interlayer space. Sabugalite in particular has the formula $(HAl(UO_2)_4(PO_4)_4.16H_2O)$ and may be written as $(H_3O)^+Al(UO_2)_4(PO_4)_4.15H_2O)$ or as $(H_9O_4)^+Al(UO_2)_4(PO_4)_4.12H_2O)$. From a chemistry point of

• Author to whom correspondence should be addressed (r.frost@qut.edu.au)

view the mineral is a protonated mineral with hydrated protons in the interlayer. It should be noted that the crystal structure of sabugalite has not been determined. The reason for this is that the energy of the X-ray beam causes the decomposition and partial dehydration of the sabugalite. Further, the structure of the thermally dehydrated products of sabugalite are unknown. Thus Raman spectroscopy can provide information on the structure of sabugalite and its dehydration products which may not be obtained by single crystal X-ray diffraction procedures or other means.

There has been considerable research in the infrared spectroscopy of the autunite minerals [4,6,7,9-12]. Few studies of the Raman spectroscopy of the autunite minerals have been forthcoming [13-16]. Pham Thi et al. studied some synthetic phases related to the autunite minerals using Raman spectroscopy. Nikanovich et al. (1976) calculated the vibrational spectrum of calcium uranyl phosphate hexahydrate and compared the calculated results with the experimentally determined values [17]. By using the structural fragment $[(UO_2)_4(PO_4)]^{5+}$ with D_{2d} symmetry. Nikanovich et al. calculated and observed wavenumbers for the ν_1 $(UO_2)^{2+}$ (A_1, B_2, E) as 822 (calculated), 820 weak (IR) and 828 strong (Raman), and for the ν_3 $(UO_2)^{2+}$ (A_1, B_2, E) 919 (calculated) and 913 (IR)) [17]. All these types (A_1, B_2, E) were described as accidental vibration degeneracy caused by the increase of the number of the degrees of freedom for the system of four identical uranyl groups in comparison with one uranyl group.

Existing data in the literature make it clear that the wavenumber which belongs to the ν_1 $(UO_2)^{2+}$ symmetric stretching mode is in most cases found in the region around 850 cm^{-1}, whereas the antisymmetric stretching mode ν_3 $(UO_2)^{2+}$ has a distinctly higher wavenumber and is situated in a region near 950 cm^{-1}. [18,19] Complications may arise because of the possibility of coupling between vibrations of different uranyl groups in cases where two or more of these are present in one and the same molecule or chain. This coupling results in splitting of bands in the vibrational spectra. Interactions between the vibrations of different molecules in the same unit cell may cause a further splitting of bands (factor group splitting), e.g. in synthetic metaschoepite possessing 4 distinct uranium atoms in the unit cell results in the following bands 840wsh, 843wsh, 847VS, 866wsh, 867wsh, 870vvs (Raman) and 856vs broad (IR). Another example is $[(UO_2)_2(OH)_2Cl_2(H_2O)_4]$, with two distinct uranium atoms in the unit cell and 847.5S, 850S, 852sh, 855vvw (Raman) and 851mS,sharp, 873sh, 883m (IR). It is apparent that there have been no post 2000 studies of the vibrational spectroscopy of the uranyl micas and few Raman spectroscopic investigations. [20-24] Čejka reported the infrared spectrum of sabugalite. [5] Čejka et al. reported the site and factor group analyses of selected uranyl micas. [9] Čejka et al. found a weak absorption band at 810 cm^{-1} and assigned this band to the ν_1 $(UO_2)^{2+}$ symmetric stretching mode. The doubly degenerate ν_2 $(UO_2)^{2+}$ splits into two components with absorption bands at 298 and 254 cm^{-1}. Two structurally distinct uranyls may be present in the crystal structure as discussed for uranyl natural and synthetic phases by Burns. [2,25]

Our interest in minerals with layered structures motivates this research as does the search for fundamental understanding of minerals that contain hydrated cations and phosphate or arsenate anions [26-29]. In this work we report the thermal transformation of sabugalite, an oxonium-aluminum based uranyl phosphate, as determined by thermo-Raman spectroscopy and by heating stage infrared spectroscopy. [30-32]

Experimental

Synthesis of Sabugalite

In order to avoid the difficulties associated with using natural samples which may have significant isomorphic substitution, a sabugalite mineral was synthesised according to the reaction:

$$4UO_2(Ac)_2 + AlCl_3 + 4H_3PO_4 \rightarrow H\,Al(UO_2)_4(PO_4)_4 + 8CH_3COO^- + 11H^+$$

Sabugalite was synthesised by the reaction of uranyl acetate and aluminium chloride in the presence of phosphoric acid as shown above. Uranyl acetate ($\{UO_2(OOCCH_3)_2.2H_2O\}$1.9339 g, 0.0043 moles) and aluminium chloride ($\{AlCl_3\}$0.145 g, 0.0011 moles)were both dissolved in ultrapure water, with final solution being 500 mL. The 2 cm^3 of phosphoric acid (85% solution, 2.873 g, 0.029 moles) was made up to 100 cm^3 with ultrapure water. The phosphoric acid solution was added dropwise to the above solution with constant stirring. Resulting suspension was left over night with gentle heating, approx 60°C, overnight. The sabugalite was removed the following morning by filtration and was then washed with pure water and air dried.

X-ray diffraction

X-Ray diffraction patterns were collected using a Philips X'pert wide angle X-Ray diffractometer, operating in step scan mode, with Cu K_α radiation (1.54052 Å). Patterns were collected in the range 3 to 90 °2θ with a step size of 0.02° and a rate of 30s per step. Samples were prepared as a randomly orientated powder on a petroleum jelly coated glass slide. Data collection and evaluation were performed with PC-APD 3.6 software. Profile fitting was applied to extract information on the microstructure and structural defects of autunite and its alteration products. The Profile Fitting option of the software uses a model that employs twelve intrinsic parameters to describe the profile, the instrumental aberration and wavelength dependent contributions to the profile.

Thermo-Raman microprobe spectroscopy

Crystals of sabugalite were oriented on the stage of an Olympus BHSM microscope, equipped with 10x and 50x objectives and part of a Renishaw 1000 Raman microscope system, which also includes a monochromator, a filter system and a Charge Coupled Device (CCD). Raman spectra were excited by a HeNe laser (633 nm) at a resolution of 2 cm^{-1} in the range between 100 and 4000
cm^{-1}. Repeated acquisition using the highest magnification was accumulated to improve the signal to noise ratio. Spectra were calibrated using the 520.5 cm^{-1} line of a silicon wafer. In order to ensure that the correct spectra are obtained, the incident excitation radiation was scrambled. Previous studies by the authors provide more details of the experimental technique [27,33-36]. Spectra at elevated temperatures or at liquid nitrogen temperature were obtained using a Linkam thermal stage (Scientific Instruments Ltd, Waterfield, Surrey, England). Spectral manipulation such as baseline adjustment, smoothing and normalisation was performed using the GRAMS® software package (Galactic Industries Corporation, Salem, NH, USA).

Infrared absorption spectroscopy

Diffuse Reflectance Fourier Transform Infrared spectroscopic (commonly known as DRIFT) analyses were undertaken using a Nicolet Nexus 870 spectrometer. 512 scans were obtained at a resolution of 2 cm^{-1} with a mirror velocity of 0.3 cm/sec. Spectra were summed to improve the signal to noise ratio. The infrared spectra were obtained by making up a KBr disc of the sabugalite, placing the disc on a polished silver reflective surface which is part of the Linkham thermal stage, and collecting reflectance spectra from the disc. This technique has been developed especially for obtaining the infrared spectra of sabugalite in the 20 to 160 °C temperature range. [30-32]

Results and discussion

X-ray diffraction

The XRD patterns of the natural and synthetic sabugalite together with the XRD patterns of the thermally treated sabugalites are shown in Figure 1. The natural sabugalite has an intense peak at 10.45 ° two theta corresponding to a d-spacing of 8.46 Å. In comparison the synthetic sabugalite shows two spacings at 9.56 and 8.67 Å. The published data gives a value of 9.63 Å. The synthetic sabugalite is apparently different to that of the natural mineral. Thermal treatment of the natural sabugalite using the high resolution thermal analysis facility results in the spacing of 8.35 Å . The spacing for the thermally treated synthetic sabugalite is 9.61 Å. which is close to the JCPDS standard for sabugalite. This sample was used for the spectroscopic analyses. It is probable that the sabugalite should be written as$((H_3O)Ca,Al)_2(UO_2)_8(PO_4)_8.32H_2O)$. The empirical oxide formula for sabugalite can be written $4UO_3:2P_2O_5:0.5Al_2O_3:16.5H_2O$ (or, equivalently, $8UO_3:4P_2O_5:Al_2O_3:33H_2O$).

Thermo-Raman microscopy of sabugalite

The Raman spectra of sabugalite at liquid nitrogen temperature are shown in Figures 2 and 3. It is not known whether the structure of sabugalite is the same at 298 K as 77 K. In all probability it is not. Other compounds of this type such as trögerite, chernikovite, meta-ankoleite undergo phase changes upon cooling. Thus the data at 77 K may not be truly representative of the data at 77 K. The reason for obtaining spectra at 77 K is to obtain better band separation so that the assignment of bands is more easily undertaken. Obtaining the Raman spectra of sabugalite at liquid nitrogen temperature seems to have differentiated between two types of phosphate units in the sabugalite structure. It is possible that the mineral underwent a phase change upon cooling to liquid nitrogen temperature. Figure 2 shows the symmetric stretching region of the $(UO_2)^{2+}$ units and Figure 3 the antisymmetric stretching region of the $(PO_4)^{3-}$ units. The results of the band component analyses are reported in Table 1. It should be noted that the ν_1 symmetric stretching mode of $(PO_4)^{3-}$ units is not activated. As a consequence no band is observed in the Raman spectrum. It would be expected that a $(PO_4)^{3-}$ stretching vibration would be observed at around 935 to 950 cm^{-1}. Such a phenomenon was also observed by Čejka et al. in the infrared spectrum [5]. In many of the autunite minerals the two UO bonds are non-equivalent as single crystal X-ray diffraction shows that two different UO bond lengths are obtained [2,25,37]. In the case of sabugalite the structure is unknown. Further the four PO bonds in the $(PO_4)^{3-}$ units are non-equivalent as determined by Raman spectroscopy. This means that there can be no in-phase vibration. The non-equivalence of the UO bonds in the $(UO_2)^{2+}$ units is reflected in the Raman spectrum at 77K. Two bands are observed at 835 and 830 cm^{-1} which are assigned to the $(UO_2)^{2+}$ stretching vibrations. The band profile is asymmetric on the lower wavenumber side and a band may be resolved through band fitting at 817 cm^{-1}. One possibility is that this band is a water librational mode. A low intensity band is observed at 895 cm^{-1} and is assigned to the ν_3 antisymmetric stretching vibration of $(UO_2)^{2+}$ units.

Five bands are observed in the 950 to 1050 cm^{-1} region in the Raman spectrum of sabugalite. These bands are assigned to the ν_3 antisymmetric stretching vibration of $(PO_4)^{3-}$ units. Čejka et al. assumed that the ν_1 and ν_2 modes in the infrared spectra of sabugalite were not infrared active even though the lowering of the symmetry from T_d to D_{2d} occurs [9]. This symmetry lowering does not cause the activation of these modes. The splitting of triply degenerate vibrations ν_3 and ν_4 (PO_4) (F2 -- E + B2) is in agreement with experimentally found values [5,6]. Very intense absorption bands at 995 and 1123 cm^{-1} belong to ν_3 (PO_4); absorption bands at 470 and 542 cm^{-1} to ν_4 (PO_4) [5,6]. The Raman spectrum at liquid nitrogen temperature shows five bands in the ν_3 antisymmetric stretching region for $(PO_4)^{3-}$ (Figure 3). The band at 1001 cm^{-1} is broad and may be decomposed into two bands which give two sets of three ν_3 bands. Obtaining the Raman spectra of sabugalite at

liquid nitrogen temperature seems to have differentiated between two types of phosphate units in the sabugalite structure. It is possible that the mineral underwent a phase change upon cooling to liquid nitrogen temperature. It is known that some of the meta-autunite group minerals meta-ankoleite, chernikovite and trögerite undergo phase transitions to lower symmetries upon cooling to low temperature. Nevertheless at liquid nitrogen temperature there is two distinct PO_4 units may be present in the crystal structure of sabugalite.

The Raman spectra of the 750 to 900 cm^{-1} region of sabugalite at selected temperatures are shown in Figure 4. The results of the band component analysis are reported in Table 3. In the Raman spectrum at 0 °C, two bands are observed at 833 and 823 cm^{-1} and are attributed to the UO_2 symmetric stretching vibrations. In the infrared spectrum of sabugalite a low intensity absorption band was observed at 810 cm^{-1}[15]. In all of the Raman spectra at any temperature, multiple UO_2 stretching modes are observed. This reflects the non-equivalence of the two uranyl bonds. In the Raman spectrum of sabugalite at 40 °C, three bands are observed at 826 (doublet) and 806 cm^{-1} with an additional low intensity band at 848 cm^{-1}. In the spectrum at 50 °C, bands are observed at 846, 829, 820 and 804 cm^{-1}. The band observed at 806 cm^{-1} in the 40 °C spectrum increases in intensity with temperature. The 826 cm^{-1} splits into two bands in the 50 °C spectrum at 829 and 820 cm^{-1}. The complexity of the UO_2 stretching region is evident in both the 60 and 80 °C spectra. The intensity of the two higher wavenumber bands at around 850 and 838 cm^{-1} increases significantly at these temperatures. The bands are observed at 849, 838, 826 and 810 cm^{-1} over the 100 to 160 °C temperature range.

According to Čejka [6], based upon the work of Veal et al. [38] and Hoekstra [39], an equation may be used to calculate the bond distances from the ν_3 stretching vibration. A band position of 895 cm^{-1} provides U-O bond lengths of 1.769 Å (using a Veal type expression) and 1.784 Å (according to Glebov [40,41]). The value of ν_1 $(UO_2)^{2+}$ of 850 cm^{-1} corresponds to a U-O bond length of 1.7618 Å, 835 cm^{-1} to 1.773 Å and 830 cm^{-1} to 1.7808 Å [42]. Table 2 shows the variation of U-O bond length with band position of the ν_1 symmetric stretching mode. A linear relationship exists between the band position (in cm^{-1}) of the ν_1 symmetric stretching mode and the U-O bond length (in Å) as is illustrated in Figure 5. [6] One possible conclusion from these intensity changes is as follows. The two bands at ~850 and 839 cm^{-1} are associated with bonding of UO_2 groups to $1/2[H_3OAl]^{4+}$ ions. Locock and Burns proposed that the Ca^{2+} is significantly under-bonded in autunite with 1.71 valence units [8]. Dehydration may force the Ca^{2+} to coordinate to the uranyl oxygens. This bonding is observed as increased intensity in the ~850 and 839 cm^{-1} bands. This means that the two UO_2 bands at ~826 and 806 cm^{-1} are associated with non-bonding or weak bonding. In the structure proposed by Locock and Burns the Ca^{2+} is bonded to two uranyl oxygens linearly at long interatomic distances of 3.275 Å. Dehydration causes the collapse of the structure and forces the Ca^{2+} to bond to the uranyl units. It is suggested a similar phenomena occurs in sabugalite. The number of vibrations proves that structurally distinct uranyls are present in the crystal structures formed during dehydration. The partial dehydration alters the structural environments of the uranyl ions such that they become non-equivalent.

Three bands are observed in the 0 °C spectrum at 1018, 1006 and 987 cm^{-1} and are attributed to the PO_4 ν_3 antisymmetric stretching vibrations (Figure 6). Čejka et al. observed two strong absorptions at 1123 and 995 cm^{-1} in the infrared spectrum of sabugalite [5]. In the spectrum at 40 °C bands are observed at 1008, 984 and 970
cm^{-1}. In the 60 °C spectrum two bands are observed at 1004 and 984
cm^{-1}. At this temperature an additional low intensity band is observed at 966 cm^{-1}. This band is assigned to the PO_4 ν_1 symmetric stretching vibration. Activation of this band only occurs after thermal treatment above 60 °C. In the spectrum at 80 °C three bands are observed at 1014, 1002 and 985 cm^{-1} and are ascribed to the PO_4 ν_3 antisymmetric stretching vibrations. Bands are found in these positions over the 80 to 100 °C temperature range.

An additional band is observed in the spectra from 100 to 140 °C at around 1060 cm^{-1}. Čejka rightly points out that fully hydrated sabugalite is uranosphatite $HAl(UO_2)_4(PO_4)_4.40\ H_2O$. $(HAl(UO_2)_4(PO_4)_4.16H_2O)$ may be written as $(H_3O)^+Al(UO_2)_4(PO_4)_4.15H_2O)$ or as $(H_9O_4)^+Al(UO_2)_4(PO_4)_4.12H_2O)$. Uranospathite may be a higher hydrate related to sabugalite, but it is not equivalent. Thus oxonium ions could be expected for this mineral. It is assumed that these types of ions would be in the interlayer. The stretching vibrations (both ν_1 and ν_3) of the $(H_3O)^+$ ions should be observed in the 2500 to 3400 cm^{-1} region [13,14,16]. The bending vibrations ν_2 and ν_4 should be observed in the 950 to 1140 and 1670 to 1750 cm^{-1} regions respectively [13,14,16]. Čejka reports the difficulty of studying these vibrational modes of $(H_3O)^+$. The stretching vibrations of $(H_3O)^+$ overlap with those of (H_2O); the bending vibration of $(H_3O)^+$ overlaps with the ν_3 modes of (PO_4) ; and the ν_4 modes of $(H_3O)^+$ overlaps with the ν_2 bending modes of (H_2O). It is predicted that these vibrational modes of $(H_3O)^+$ will be both Raman and infrared active. One possibility is that the additional band observed at 1062 cm^{-1} is the Raman active ν_2 bending mode of $(H_3O)^+$.

The infrared spectra of the water OH stretching region of thermally treated sabugalite as a function of temperature are shown in Figure 7. At 20 °C, four bands are observed at 3597, 3433, 3226 and 3069 cm^{-1}. The first three bands are attributed to the OH stretching vibrations of water. In all the spectra shown in Figure 8, a broad band is observed around 3069 cm^{-1}. It is proposed that this band may be attributed to the stretching vibrations of $(H_3O)^+$. The results of the band component analysis of the hydroxyl stretching region are reported in Table 3. The fitting of the spectral profile of the OH stretching region is consistent. Some variation in the position of the fourth band is noted; however this may be a function of the fitting of the baseline. The intensity of the bands 3 and 4 decrease with increased temperature.

Studies have shown a strong correlation between OH stretching frequencies and both O···O bond distances and H···O hydrogen bond distances [43-46]. Libowitzky (1999), based upon the hydroxyl stretching frequencies as determined by infrared spectroscopy, showed that a regression function can be employed relating the above correlations with regression coefficients better than 0.96 [47].
The function is $\nu_1 = 3592\text{-}304x109exp(\text{-}d(O\text{-}O)/0.1321)\ cm^{-1}$. By using this formula the band at 3069 cm^{-1} provides an OH.O hydrogen bond distance of 2.66_{58} Å; the band at 3226 cm^{-1} a hydrogen bond distance of 2.71_3 Å, the band at 3433 cm^{-1} a bond distance of 2.82_3 Å. The band at 3596 cm^{-1} results from large hydrogen bond distances and the Libowitzky type calculation does not work for these types of hydroxyl stretching high wavenumbers. At this point in time no single crystal studies of sabugalite either synthetic or natural have been forthcoming; as a consequence a comparison of bond distances between X-ray crystallographic data and infrared spectral results cannot be undertaken. Some conclusions may be made: the hydrogen bond distances of $(H_3O)^+$ are shorter than those of H_2O. Thus the $(H_3O)^+$ forms stronger hydrogen bonds than does H_2O. The observation of three hydroxyl stretching band positions shows that there are three hydrogen bonds formed with different bond strengths and is related to the positions of the water molecules in the sabugalite structure.

Confirmation of the existence of water with different hydrogen bond strengths is obtained by the study of the water HOH bending modes. The infrared spectral profile may be curve resolved into two components at 1629 and 1662 cm^{-1}. The first band may be attributed to weakly hydrogen bonded water such as water hydrogen bonding to adjacent water molecules in the sabugalite structure. The second high wavenumber band is attributed to strongly hydrogen bonded water as is found in the hydration sphere of cations. Čejka et al. suggested that the ν4 bending modes of $(H_3O)^+$ should be found in the 1700 to 1750 cm^{-1} region [5,13,14,16]. No infrared bands were found in this region. Čejka et al also found no bands in this region using KBr discs of sabugalite. However bands were found when the infrared analysis was undertaken using a Nujol mull technique [5]. Pham

Thi et al. also found bands at 1730 cm^{-1} for synthetic hydrogen uranyl phosphates using the Nujol method [13,14]. In agreement with the results presented here, these authors also showed strong asymmetry of the water HOH ν_2 bending mode with peak maxima in the 1650 to 1660 cm^{-1} region.

Conclusions

Thermo-Raman spectroscopy has been used to follow the changes in structure during the dehydration of sabugalite. Temperatures for the Raman spectroscopic analysis were selected based upon the thermogravimetric analysis of sabugalite. These Raman spectra were then used to characterise the changes in the molecular structure of the sabugalite. Such changes are significant since X-ray diffractions studies cause sample decomposition. Very significant changes in the Raman spectra were obtained. The crystal structure of sabugalite is unknown but may be similar to other autunite minerals with a distorted tetragonal structure. This distortion was brought about by the hydrogen bonding of the water molecules to the PO_4 and UO_2 units. The loss of water between 60 and 70 °C results in the removal of this distortion resulting in simpler Raman spectra. Further dehydration above 100 °C results in the loss of the layer structure, resulting in increased complexity in the Raman spectra. Dehydration of the mineral is readily followed by the changes in the spectra of the hydroxyl stretching region.

One of the difficulties in assigning the bands of the autunite minerals is the overlap of the stretching vibrations of the UO_2 and PO_4 and/or AsO_4 units. The AsO_4 and UO_2 stretching vibrations occur in almost identical positions. The further complexity is introduced because of the distorted structure of the sabugalite unit cell. This results in a reduction in symmetry, with several bands being found in the PO_4 antisymmetric stretching region. In the structure of sabugalite the four PO bonds are non-equivalent brought about by the non-equivalence of the two UO_2 bonds. Such non-equivalence results in the lack of intensity of the ν_1 PO_4 stretching band. This band only becomes observed after the initial dehydration steps which results in the removal of the distorted tetragonal structure.

No symmetric stretching vibration is observed until after significant dehydration has occurred at 75 °C, when a low intensity band at 927 cm^{-1} is observed. The complexity that is observed in the ν_3 antisymmetric stretching region of the PO_4 units is also observed in the PO_4 ν_2 bending region. Four bands are observed at 471, 446, 405 and 376 cm^{-1}. The loss of degeneracy is removed by dehydration and the four bands become two bands after dehydration suggesting the increased symmetry upon dehydration. It is possible that dehydration causes a displacement of the layers in the sabugalite upon thermal treatment. The structure of sabugalite is such that the two UO bonds are non-equivalent. These results in the observation of two UO stretching bands observed at 843 and 827 cm^{-1}. A low intensity band is observed at around 894 cm^{-1} and is attributed to the UO_2 antisymmetric stretching vibration. A complex set of bands is observed in the low wavenumber region. These bands are assigned to the UO_2 bending vibrations. Bands are observed at 283, 234, 218 and 196 cm^{-1} and are all assigned to UO_2 bending modes. The complexity of the UO_2 bending modes is observed up to 250 °C. This complexity is lost only after dehydration.

Acknowledgements

The financial and infra-structure support of the Queensland University of Technology Inorganic Materials Research Program of the School of Physical and Chemical Sciences is gratefully acknowledged. The Australian Research Council (ARC) is thanked for funding. Dr Llew Rintoul is thanked for technical assistance in the collection of the infrared data.
Mr Ross Pogson of the Australian museum is thanked for the loan of several of the sabugalite minerals. Mr Dermot Henry of Museum Victoria is thanked for the loan of a collection of uranyl micas including sabugalite. Professor Jiři Čejka is especially thanked for many useful and interesting discussions.

References:

1. Isobe, H, Ewing, RC, Murakami, T. *Materials Research Society Symposium Proceedings* 1994**; 333**: 653.
2. Burns, P. *Reviews in mineralogy Vol 38* 1999**; 38**: 23.
3. Cejka, J, Cejka, J, Jr., Muck, A. *Thermochimica Acta* 1985**; 86**: 387.
4. Cejka, J, Jr., Muck, A, Cejka, J. *Neues Jahrbuch fuer Mineralogie, Monatshefte* 1985: 115.
5. Cejka, J, Urbanec, Z, Cejka, J, Jr., Ederova, J, Muck, A. *Journal of Thermal Analysis* 1988**; 33**: 395.
6. Cejka, J. *Reviews in mineralogy* 1999**; 38**.
7. Muck, A, Cejka, J, Jr., Cejka, J, Urbanec, Z. *Sbornik Vysoke Skoly Chemicko-Technologicke v Praze, B: Anorganicka Chemie a Technologie* 1986**; B 31**: 71.
8. Locock, AJ, Burns, PC. *American Mineralogist* 2003**; 88**: 240.
9. Cejka, J, Jr., Muck, A, Cejka, J. *Physics and Chemistry of Minerals* 1984**; 11**: 172.
10. Gevork'yan, SV, Povarennykh, AS. *Mineralogicheskii Zhurnal* 1980**; 2**: 29.
11. Omori, K, Seki, T. *Ganseki Kobutsu Kosho Gakkaishi* 1960**; 44**: 7.
12. Urbanec, Z, Cejka, J. *Casopis Narodniho Muzea v Praze, Rada Prirodovedna* 1979**; 148**: 16.
13. Pham Thi, M, Velasco, G, Colomban, P, Novak, A. *Solid State Ionics* 1983**; 9-10**: 1055.
14. Pham-Thi, M, Colomban, P, Novak, A. *Journal of Physics and Chemistry of Solids* 1985**; 46**: 493.
15. Pham Thi, M, Colomban, P. *Solid State Ionics* 1985**; 17**: 295.
16. Pham-Thi, M, Colomban, P. *Journal of the Less-Common Metals* 1985**; 108**: 189.
17. Nikanovich, MV, Novitskii, GG, Kobets, LV, Kolevich, TA, Sikorskii, VV, Umreiko, DS. *Koordinatsionnaya Khimiya* 1976**; 2**: 253.
18. Prins, G. Uranyl chloride, its hydrates, and basic salts; React. Centrum Nederland,Petten,Neth. FIELD URL:, 1973; pp. 115 pp.
19. Prins, G, Cordfunke, EHP. *Journal of Inorganic and Nuclear Chemistry* 1975**; 37**: 119.
20. Bagnall, KW, Wakerley, MW. *Journal of Inorganic and Nuclear Chemistry* 1975**; 37**: 329.
21. Biwer, BM, Ebert, WL, Bates, JK. *Journal of Nuclear Materials* 1990**; 175**: 188.
22. Bukalov, SS, Vdovenko, VM, Ladygin, IN, Suglobov, DN. *Zhurnal Prikladnoi Spektroskopii* 1970**; 12**: 341.
23. Bullock, JI. *Journal of the Chemical Society [Section] A: Inorganic, Physical, Theoretical* 1969**; 5**: 781.
24. Maya, L, Begun, GM. *Journal of Inorganic and Nuclear Chemistry* 1981**; 43**: 2827.
25. Burns, PC, Miller, ML, Ewing, RC. *Canadian Mineralogist* 1996**; 34**: 845.
26. Martens, W, Frost, RL, Williams, PA. *Journal of Raman Spectroscopy* 2003**; 34**: 104.
27. Martens, WN, Frost, RL, Kloprogge, JT, Williams, PA. *American Mineralogist* 2003**; 88**: 501.
28. Frost, RL, Kloprogge, T, Weier, ML, Martens, WN, Ding, Z, Edwards, HGH. *Spectrochimica Acta, Part A: Molecular and Biomolecular Spectroscopy* 2003**; 59**: 2241.
29. Frost, RL, Weier, ML, Martens, W, Kloprogge, JT, Ding, Z. *Thermochimica Acta* 2003**; 403**: 237.
30. Pracht, G, Lange, N, Lutz, HD. *Thermochimica Acta* 1997**; 293**: 13.
31. Pracht, G, Weckler, B, Lutz, HD. *Applied Spectroscopy* 2003**; 57**: 1254.
32. Lutz, HD, Haeuseler, H. *Journal of Molecular Structure* 1999**; 511-512**: 69.
33. Frost, RL, Martens, W, Williams, PA, Kloprogge, JT. *Journal of Raman Spectroscopy* 2003**; 34**: 751.
34. Frost, RL, Weier, ML. *Thermochimica Acta* 2003**; 406**: 221.
35. Frost, RL, Weier, ML. *Journal of Raman Spectroscopy* 2003**; 34**: 776.
36. Martens, WN, Frost, RL, Williams, PA. *Neues Jahrbuch fuer Mineralogie, Monatshefte* 2003: 337.

37. Vochten, R, Pelsmaekers, J. *Physics and Chemistry of Minerals* 1983**; 9**: 23.
38. Veal, BW, Lam, DJ, Carnall, WT, Hoekstra, HR. *Physical Review B: Solid State* 1975**; 12**: 5651.
39. Hoekstra, HR. *Inorg. Chem.* 1963**; 2**: 492.
40. Glebov, VA. *Khimiya Urana, M.* 1989: 68.
41. Glebov, VA. *Koordinatsionnaya Khimiya* 1981**; 7**: 388.
42. Bartlett, JR, Cooney, RP. *Journal of Molecular Structure* 1989**; 193**: 295.
43. Emsley, J. *Chemical Society Reviews* 1980**; 9**: 91.
44. Lutz, H. *Structure and Bonding (Berlin, Germany)* 1995**; 82**: 85.
45. Mikenda, W. *Journal of Molecular Structure* 1986**; 147**: 1.
46. Novak, A. *Structure and Bonding (Berlin)* 1974**; 18**: 177.
47. Libowitsky, E. *Monatschefte fÜr chemie* 1999**; 130**: 1047.

Table 1 Raman spectroscopic analysis of sabugalite at elevated temperatures

	77K	0 °C	40 °C	50 °C	60 °C	80 °C	100°C	120°C	140°C	220°C	Suggested assignment
Band centre/cm^{-1}	1030						1060	1060	1062	1059	PO_4 ν_3
Bandwidth/cm^{-1}	7.9						12.5	12.5	14.2	30.0	antisymmetric
Relative Intensity/%	5						0.5	0.5	1.9	5.1	stretching??
Band centre/cm^{-1}	1022										PO_4 ν_3
Bandwidth/cm^{-1}	6.3										antisymmetric
Relative Intensity/%	2.1										stretching
Band centre/cm^{-1}	1012	1018			1014	1014	1013	1016	1019	1019	PO_4 ν_3
Bandwidth/cm^{-1}	9.6	15.3			29.5	28.5	28.3	21.7	13.0	19.8	antisymmetric
Relative Intensity/%	17.6	3.7			14.6	12.6	11.5	6.1	2.3	3.9	stretching
Band centre/cm^{-1}	1001	1006	1008	1004	1002	992	1002	1001			PO_4 ν_3
Bandwidth/cm^{-1}	22.4	23.2	24.2	26.4	12.8	48.8	7.8	20.4			antisymmetric
Relative Intensity/%	22.4	39.2	40.9	39.4	12.1	23.3	1.6	10.7			stretching
Band centre/cm^{-1}	987	987	984	984	985	990	988	987	990	989	PO_4 ν_3
Bandwidth/cm^{-1}	14.0	14.9	11.6	14.9	20.8	11.7	25.2	23.7	25.1	23.9	antisymmetric
Relative Intensity/%	12.7	10.4	10.6	13.3	23.3	19.5	28.7	23.3	39.1	39.0	stretching
Band centre/cm^{-1}		981	970								PO_4 ν_3
Bandwidth/cm^{-1}		22.6	22.7								antisymmetric
Relative Intensity/%		5.4	5.8								stretching
Band centre/cm^{-1}				966	963	962	962	962	962		PO_4 ν_1
Bandwidth/cm^{-1}				17.5	15.2	14.7	20.8	28.4	24.1		symmetric
Relative Intensity/%				5.0	8.1	7.8	7.7	9.7	2.3		stretching
Band centre/cm^{-1}				892	892	900	895	895	892	945	UO_2
Bandwidth/cm^{-1}				10.2	10.2	23.3	15.3	15.3	27.0	18.1	antisymmetric
Relative Intensity/%				0.47	0.47	0.74	0.84	0.84	1.7	1.0	stretching

Band centre/cm^{-1}			848	846	849	850	849	850	849	850	UO_2
Bandwidth/cm^{-1}			17.5	15.8	12.8	10.8	14.0	14.1	14.4	13.2	symmetric
Relative Intensity/%			0.85	6.8	3.5	10.0	6.8	3.2	4.9	5.9	stretching
Band centre/cm^{-1}	835	833		829	832	838	837	838	837	836	UO_2
Bandwidth/cm^{-1}	10.9	11.3		10.9	20.2	14.7	12.7	12.5	12.5	12.9	symmetric
Relative Intensity/%	11.7	18.4		10.6	10.2	22.5	8.2	5.6	12.0	12.8	stretching
Band centre/cm^{-1}	830	823	826	820	821	822	821	821	826	826	UO_2
Bandwidth/cm^{-1}	8.4	22.8	16.3	10.1	8.5	12.5	15.3	22.3	11.0	10.7	symmetric
Relative Intensity/%	24.5	22.7	26.7	10.1	10.0	11.6	19.3	23.7	11.7	9.3	stretching
Band centre/cm^{-1}	816		806	804	805	805	804	805	810	810	UO_2
Bandwidth/cm^{-1}	19.9		12.6	12.6	12.6	10.3	10.1	11.9	14.7	16.2	symmetric
Relative Intensity/%	3.8		10.3	13.3	16.0	4.3	8.2	5.5	22.3	23.4	stretching
Band centre/cm^{-1}				770	760	735	735	740	734		Water
Bandwidth/cm^{-1}				39.7	37.6	32.7	32.7	36.5	31.0		librational
Relative Intensity/%				1.2	1.4	1.3	1.3	1.9	1.6		

Temperature /°C	Band position /cm^{-1}	Predicted U-O bond length/ Å +/- 0.0001
0 °C	833	1.7779
	823	1.7877
40 °C	848	1.7637
	826	1.7847
	806	1.8047
50 °C	846	1.7656
	829	1.7818
	820	1.7906
	804	1.8067
100 °C	849	1.7628
	838	1.7732
	810	1.8006

Table 2 Band positions of the symmetric stretching mode and the U-O bond lengths.

Temperature	Band 1	Band 2	Band 3	Band 4
20 °C	3596	3433	3226	3069
30 °C	3600	3433	3216	3069
40 °C	3602	3437	3231	3057
50 °C	3605	3433	3221	3112
60 °C	3608	3435	3221	3131
70 °C	3609	3439	3230	3090
80 °C	3610	3439	3224	3130
90 °C	3605	3439	3216	3167
100°C	3603	3442	3219	3130
120°C	3606	3443	3225	3151
140°C	3609	3462	3253	3035

Table 3 Band positions of the water OH stretching vibrations of sabugalite as a function of temperature.

List of Figures

List of Tables

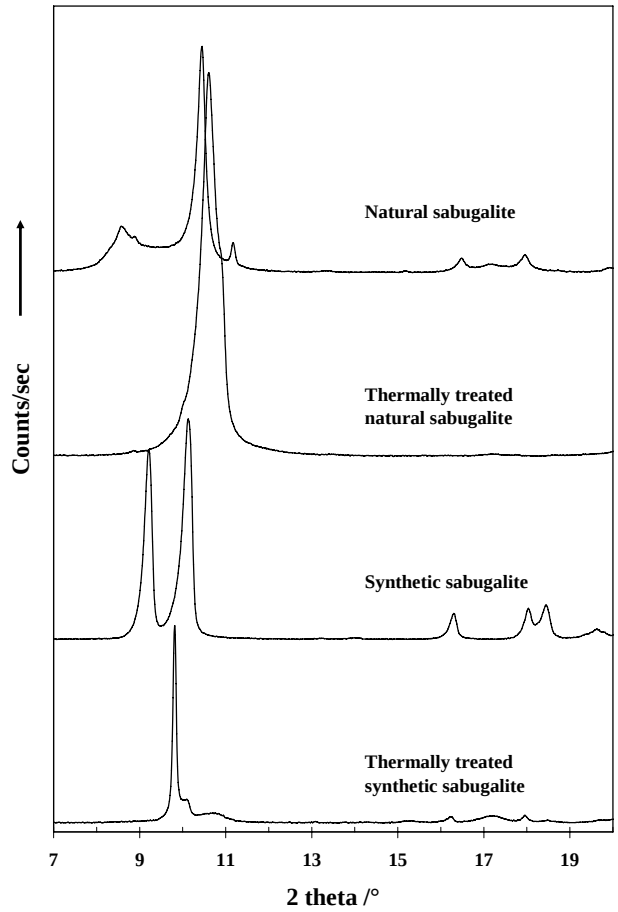

Figure 1

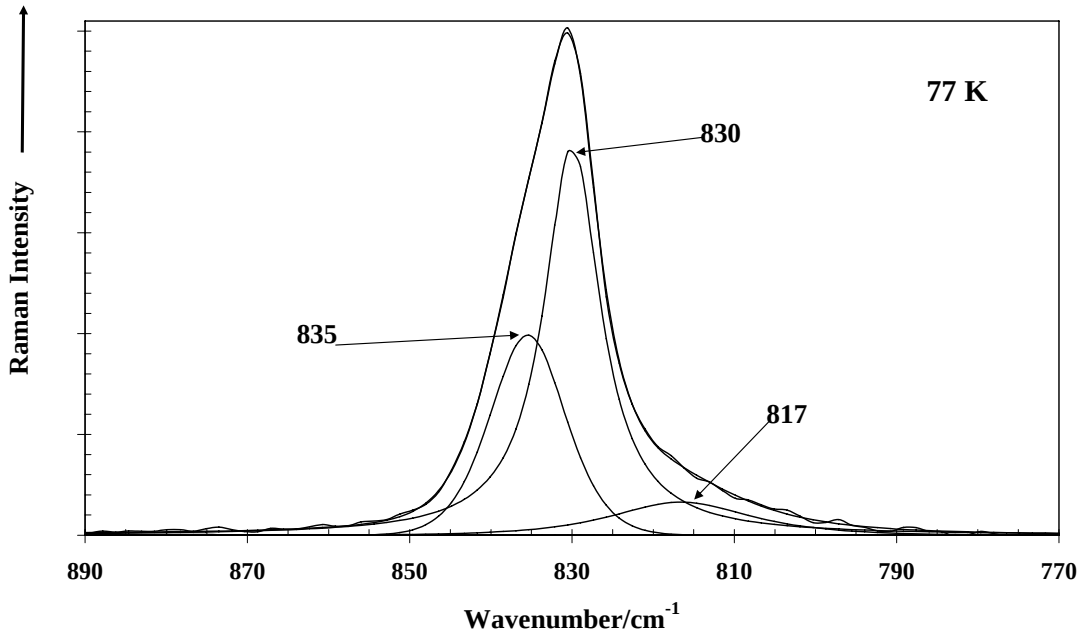

Figure 2

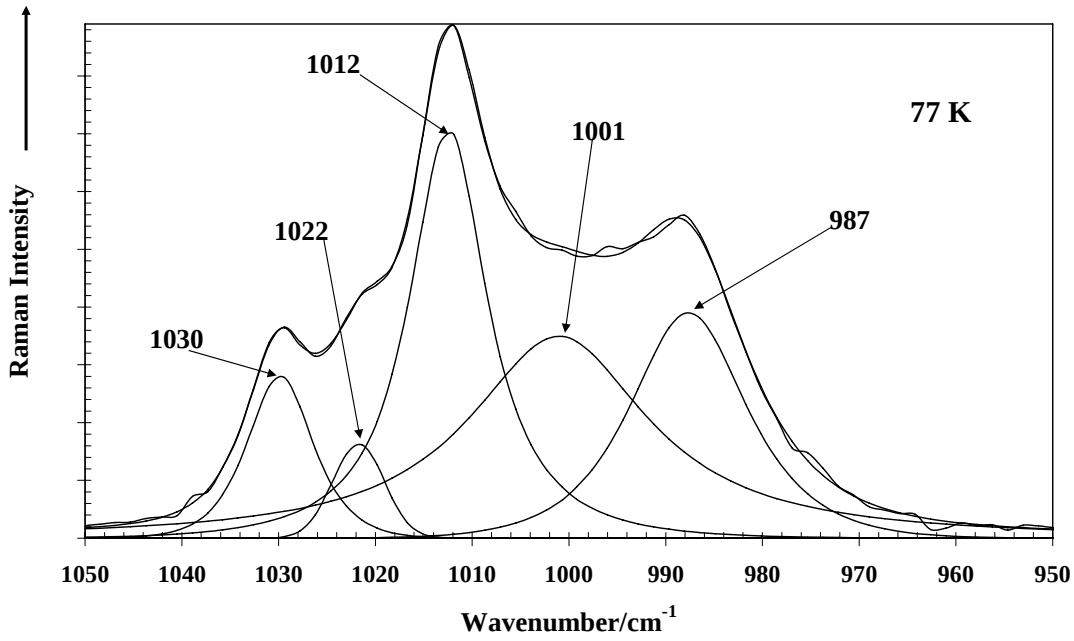

Figure 3

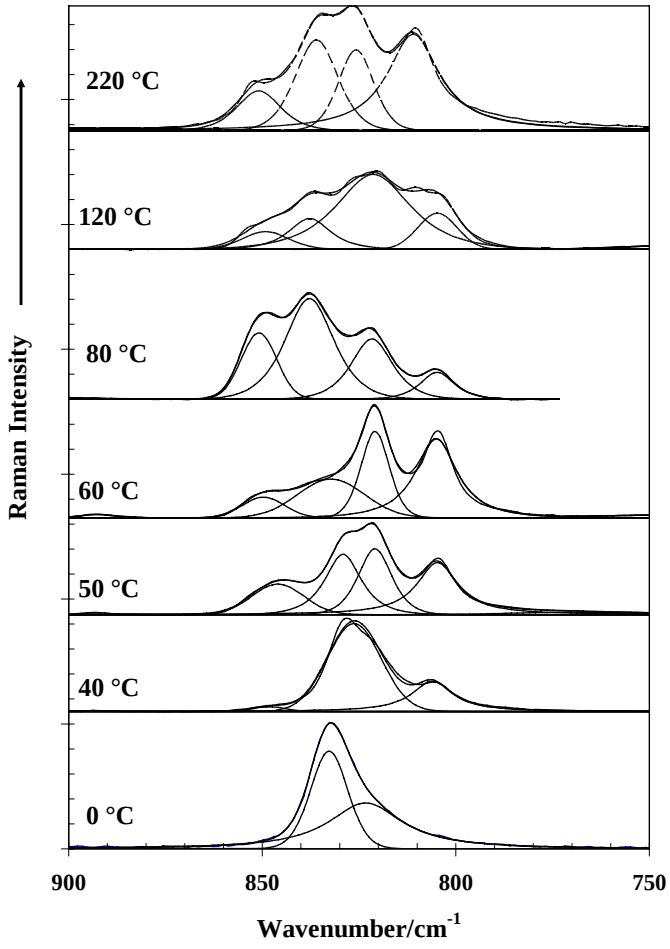

Figure 4

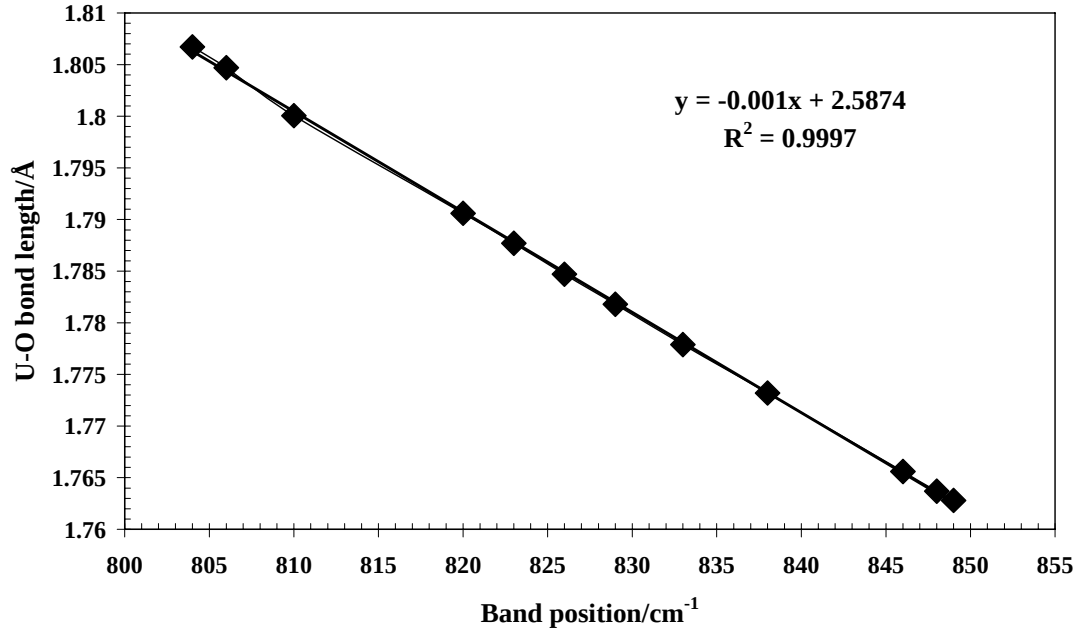

Figure 5

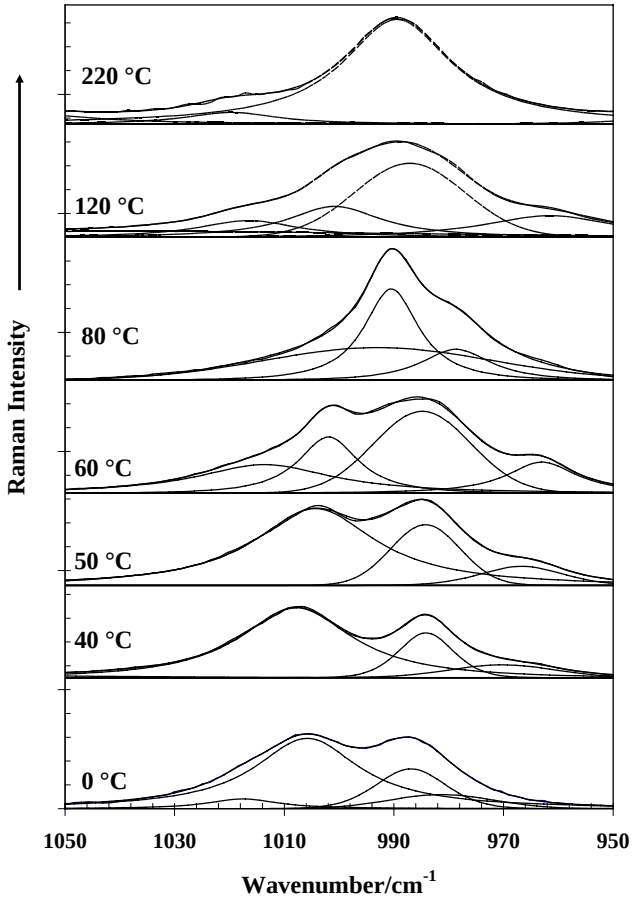

Figure 6

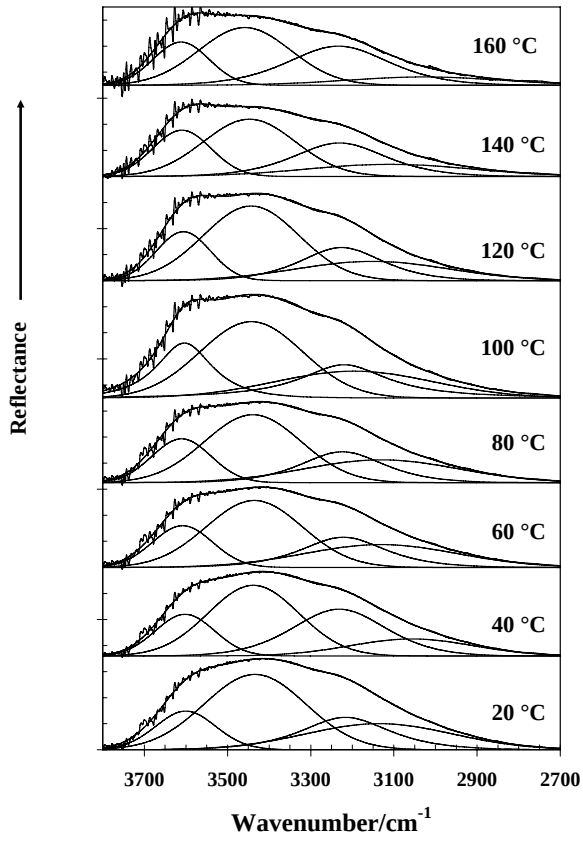

Figure7

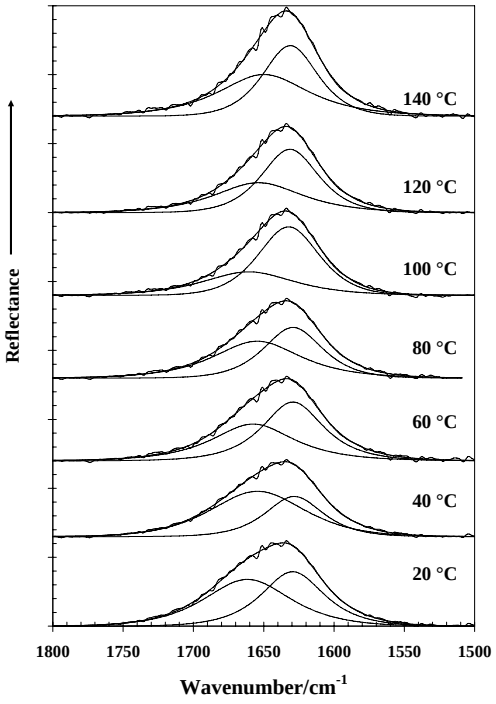

Figure 8